Increased Solubility, Liquid-Crystalline Phase, and Selective Functionalization of Single-Walled Carbon Nanotube Polyelectrolyte Dispersions

Chengmin Jiang,[†,‡,#] Avishek Saha,[†,‡,#] Changsheng Xiang,[†,‡] Colin C. Young,[‡,§,⊥] James M. Tour,[†,‡,∥] Matteo Pasquali,[†,‡,⊥] and Angel A. Martí[†,‡,¶,*]

[†]Department of Chemistry, [‡]Richard E. Smalley Institute for Nanoscale Science and Technology, [§]Applied Physics Program, [⊥]Department of Chemical and Biomolecular Engineering, [∥]Department of Mechanical Engineering and Materials Science, and [¶]Department of Bioengineering, Rice University, Houston, Texas 77005, United States. [#]These authors contributed equally.

ABSTRACT The solubility of single-walled carbon nanotube (SWCNT) polyelectrolytes $[K(THF)]_n$SWCNT in dimethyl sulfoxide (DMSO) was determined by a combination of centrifugation, UV−vis spectral properties, and solution extraction. The SWCNT formed a liquid crystal at a concentration above 3.8 mg/mL. Also, crown ether 18-crown-6 was found to increase the solubility of the SWCNT polyelectrolytes in DMSO. Raman spectroscopy and near-infrared (NIR) fluorescence analyses were applied to study the functionalization of SWCNTs. Small-diameter SWCNTs were found to be preferentially functionalized when the SWCNT polyelectrolytes were dispersed in DMSO.

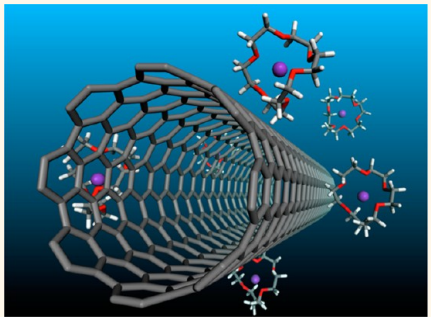

KEYWORDS: SWCNT polyelectrolytes · crown ethers · liquid crystal · diameter selectivity

Homogeneous dispersion of single-walled carbon nanotubes (SWCNTs) is still a highly active field of research. While individual SWCNTs have amazing electronic and mechanical properties with potential applications in thin film transistors,[1,2] conductive films,[3−6] and organic photovoltaics,[7,8] the construction of devices based on SWCNTs requires, as a first step, their disentanglement and individualization.[9] To exploit the outstanding properties of individualized SWCNTs, one has to overcome the formidable van der Waals attractions among tubes (0.5 eV/nm),[10] which is the main obstacle to make uniform and stable dispersions. Over the past few years, many effective dispersion technologies have been developed, including covalent sidewall functionalization,[11−13] noncovalent interaction-assisted dispersion,[14−16] and superacid dissolution.[9,17−19] Another intriguing way to disperse SWCNTs is by forming SWCNT polyelectrolytes, where nanotubes are negatively charged by reduction by alkali metals. Upon adding polar aprotic solvents, the negatively charged sidewalls of the nanotubes induce Coulombic repulsion between tubes, resulting in their spontaneous dissolution.[20−22] Early work in this field showed that SWCNT polyelectrolytes can be synthesized by metallic lithium reduction.[23,24] Later, Pénicaud reported the use of other alkali metals and showed that SWCNT salts $[A(THF)]_n$CNT (A = Li, Na, K) could spontaneously dissolve in a series of aprotic organic solvent, such as dimethyl sulfoxide (DMSO) and sulfolane.[20−22] However, the reported solubility of HiPco SWCNT polyelectrolytes was relatively low (0.4 mg/g in DMSO), which prevents the formation of a liquid crystal and limits its further processing into macroscopic assembly such as SWCNT fibers or sheets.[20]

The manufacture of SWCNT dispersions into aligned macroscopic materials by spinning or coagulation[18,25−28] requires a preorganization of the carbon nanotubes' solutions into a liquid-crystalline phase. Important applications have been devised for SWCNTs' liquid-crystal phases such as the formation of fibers made of highly aligned SWCNTs,[28]

* Address correspondence to amarti@rice.edu.

Received for review March 6, 2013 and accepted April 5, 2013.

Published online April 16, 2013
10.1021/nn4011544

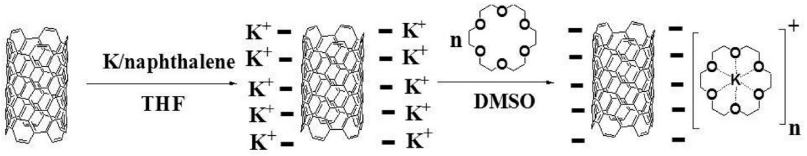

Scheme 1. Idealized representation of crown-ether-assisted dissolution of SWCNT polyelectrolyte.

thin film transistors made of highly oriented carbon nanotube arrays,[25] 3-D photonic devices,[29] and the fractionation of carbon nanotubes by length.[30] The formation of nematic phases in other SWCNT dispersion systems, such as dispersions in superacid and by noncovalent interaction (surfactants and DNA), is possible when the concentration of SWCNTs is sufficiently high.[18,31−33] However, to the best of our knowledge, the formation of liquid-crystalline phases has never been reported for SWCNT polyelectrolytes. The reason for this is probably related to the insufficient solubility of SWCNT polyelectrolyte dispersions in previous reports. The use of SWCNT polyelectrolyte liquid-crystal dispersion for the production of ordered macroscopic materials is attractive due to the convenient chemical properties of SWCNT polyelectrolytes. For example, alkyl bromides are known to readily react with SWCNT polyelectrolytes to form alkyl-functionalized carbon nanotubes.[24] In this report, we study the dependence of the initial amount of SWCNT polyelectrolyte and the presence of a cation sequester (18-crown-6) on the solubility of SWCNT polyelectrolytes (Scheme 1). We also demonstrate that a liquid-crystalline phase can be detected at concentrations of 3.8 mg/mL of SWCNT polyelectrolytes. Finally, we examine how the diameters of different SWCNTs influence their solubility and reactivity.

RESULTS AND DISCUSSION

Probing the Solubility of SWCNT Polyelectrolytes. Different amounts of the SWCNT salt were added to DMSO inside a nitrogen-purged glovebox, stirred overnight, and centrifuged. The supernatant layers were then removed, and the solubilities of the SWCNT polyelectrolytes were determined from the UV−vis absorption intensity at 500 nm using a proportionality constant (Supporting Information, Figure S1). This proportionality constant was calculated by drying a measured volume of the supernatant and weighing the residue following a previously reported method.[22] Using this procedure, we calculated a proportionality constant of 3.23×10^{-3} ppm^{-1} mm^{-1} (0.323 mL/mg mm^{-1}), which was used to calculate the concentration of SWCNTs in all solutions. Figure 1 shows the concentration of SWCNT polyelectrolytes in DMSO solution as a function of the concentration of material in the initial mixture. Interestingly, we found that the solubility of the SWCNT polyelectrolytes was highly dependent on the initial amount of the materials in DMSO. It is noticeable that two different regions can be observed in the graph. There is a region where the concentration of SWCNT polyelectrolytes increases linearly up to an initial concentration near 3 mg/mL. This linear increase indicates a constant mass percent conversion of 10.6%, similar to the mass percent conversion of up to 9.4% in SWCNT dispersions with surfactants observed by Smalley group.[34]

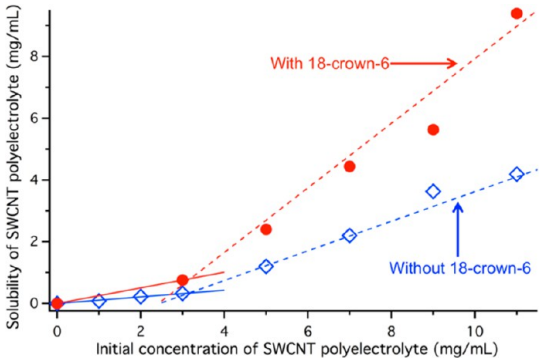

Figure 1. Concentration of HiPco SWCNT polyelectrolytes in DMSO at different initial concentrations. Open blue diamonds and the solid red circles represent SWCNTs without and with crown ether, respectively. Each curve exhibits a change in slope at 3 mg/mL initial concentration; solid and dashed lines indicated best linear fits to the data above and below this concentration.

Increasing the initial concentration above 3 mg/mL causes a change in the curve slope. The concentration of SWCNT polyelectrolytes appears also to increase linearly with the initial concentration, but in this case, the slope is larger, making for a mass percent conversion of 52%. These two distinct regions in Figure 1 are consistent with the transition from an isotropic phase, where SWCNTs are randomly oriented in solution, to a biphasic region, where a nematic liquid-crystalline phase is in equilibrium with the isotropic phase. The better packing of one-dimensional structures such as SWCNTs in the liquid-crystalline phase is likely to be responsible for larger mass percent conversion of SWCNT polyelectrolytes at higher initial concentrations.

Cation condensation onto the surface of negatively charged SWCNTs has been claimed as one of the main reasons for the limited solubility of SWCNT polyelectrolytes.[22] Crown ethers are known for their extraordinary ability to coordinate alkali metal ions, hence shielding their charge from their counterions and solvent, and resulting in a higher distance between the ion pairs.[35] Dissolution of alkali metal salts in organic solvents has been possible by trapping the

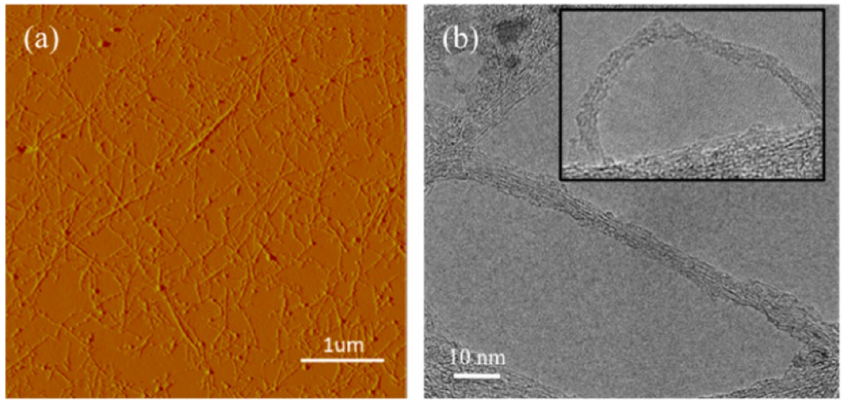

Figure 2. (a) AFM image of HiPco SWCNT polyelectrolytes deposited on fused silica from supernatant solution (0.26 mg/mL) in DMSO. (b) TEM images of HiPco SWCNT polyelectrolytes in Formvar grid showing small bundles (inset is a different image with the same scale bar).

metal cation with crown ethers.[36,37] Taking these facts into consideration, we studied the effect of crown ethers on the solubility of SWCNT polyelectrolytes. The crown ether 18-crown-6 was selected due to its high affinity for potassium cations. The red circles in Figure 1 show also a linear increase in solubility of SWCNT polyelectrolytes in DMSO in the presence of the crown ether 18-crown-6. Supporting Information Figure S3 shows a representative curve in which the solubility of a 5 mg/mL SWCNT polyelectrolyte solution is plotted as a function of 18-crown-6 concentration. The figure shows that, as the amount of 18-crown-6 increases, the solubility of the SWCNT polyelectrolytes grows continuously up to a maximum which is attained between 15 and 20 mg/mL of the crown ether. Interestingly, we were able to obtain concentrations of SWCNT polyelectrolytes up to 9.4 mg/mL (initial concentration of SWCNTs 11 mg/mL), which exceeds all previous reported solubilities for SWCNT polyelectrolytes (the highest solubility ever reported for the HiPco SWCNT polyelectrolyte is 0.4 mg/g in DMSO[20] and for Arc SWCNT polyelectrolyte is 4.3 mg/mL in DMSO[22]).

Pénicaud and co-workers built a model for the SWCNT polyelectrolyte dispersions as soluble polyelectrolytes, which strikingly captures our experiment results. The highest reported solubility from this group was 4.3 mg/mL, although their model predicts solubility up to 10 mg/mL. They attributed this discrepancy to nanotube−nanotube interactions.[22] In our case, the addition of 18-crown-6 to the mixture captures the potassium cations, which prevents the condensation of the counterions and increases the charge−charge repulsion among nanotubes, thus increasing the amount of SWCNT polyelectrolyte in solution up to 120%. However, the supernatant layer showed increased viscosity with concentration, which resulted in the formation of a gel at concentrations larger than 9.4 mg/mL, even when the solution is kept under a blanket of dry nitrogen (Figure S4). Higher concentrations of carbon nanotubes in DMSO form dense gels immediately, preventing the precise determination of their solubility.

Characterization of the SWCNT Polyelectrolyte Dispersions in DMSO. Figure 2a shows an atomic force microscopic image of HiPco SWCNT polyelectrolyte dispersions (10 times diluted from 2.6 mg/mL) in DMSO dip-coated on a fused silica surface and dried in vacuum in 100 °C for 1 h, showing that almost all of the SWCNTs dispersed are isolated or in small bundles. Similarly, the TEM in Figure 2b shows a small SWCNT bundle (*ca.* 5−6 nm). The presence of small bundles is likely a consequence of sample preparation for the microscopy experiment. Samples prepared for microscopy become unavoidably exposed to air and moisture when they are being transferred to the microscope.

Because we can dissolve relatively high concentrations of individually dispersed SWCNTs in DMSO, we investigated evidence of liquid-crystalline behavior. As expected, the relatively concentrated solutions of SWCNT polyelectrolytes form liquid-crystalline phases. Polarized microscope optical images clearly show the birefringence associated with the formation of liquid-crystal phases when the SWCNT concentration exceeds 3.8 mg/mL (Figure 3a,b). It is important to note how the image brightness changes when the sample is rotated relative to the polarizers. Samples with lower concentrations of SWCNTs did not show birefringence under cross-polarizers (see Supporting Information, Figure S5). To the best of our knowledge, this is the first report of a liquid-crystal state obtained from SWCNT polyelectrolytes. Although the region delimited by the dashed lines in Figure 1 suggests that lower concentration of SWCNTs could also present liquid-crystalline behavior, we were not able to see birefringence in samples with concentrations of 2.3 mg/mL. This may be due to the small amount of liquid-crystalline phase expected at these low concentrations.

The polarized microscopy optical image in Figure 3c,d demonstrates that the addition of 18-crown-6 does not disturb the formation of the liquid-crystalline phase.

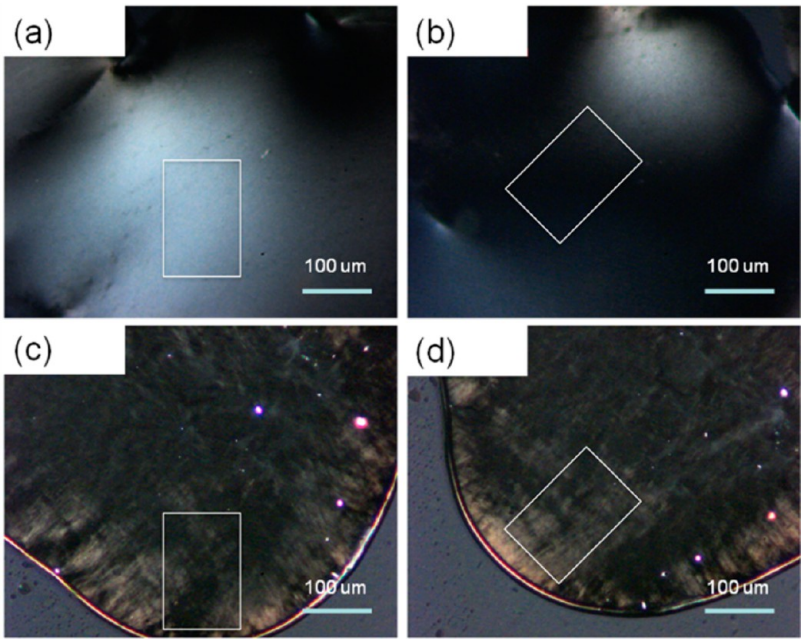

Figure 3. Polarized optical image of supernatant layers of 3.8 mg/mL HiPco SWCNT polyelectrolytes imaged under cross-polarizers with the stage rotated at (a) 0° and (b) 45°. Polarized optical image of 4.4 mg/mL HiPco SWCNT polyelectrolytes with 20 mg/mL crown ether imaged under cross-polarizers with the stage rotated at (c) 0° and (d) 45°. The round edges demark the edges of a droplet.

It should be noted that the brightness of Figure 3c,d is diminished due to the higher concentration of SWCNTs (and therefore higher light absorption) caused by the presence of crown ether. Nonetheless, the image shows changes in brightness when the stage is rotated, consistent with a liquid-crystalline phase. Therefore, the presence of crown ether in the SWCNT polyelectrolyte dispersions could be quite useful to increase the solubility and to obtain the liquid-crystalline phase.

Diameter-Dependent Chemical Functionalization in SWCNT Polyelectrolyte Dispersions. To better understand the SWCNT polyelectrolyte solutions, we used methanol to quench the supernatant and the residue after initial dispersion in DMSO and characterized the material using Raman and NIR photoluminescence spectroscopy. Figure 4a shows the Raman spectra of different SWCNT preparations in the G and D peak regions. Pristine SWCNTs and SWCNT polyelectrolyte solid salts quenched with methanol show similar features, with a slight increase in the D band for the SWCNT-quenched polyelectrolyte solid. This increase in the D band can be attributed to hydrogenation, *via* anion protonation, of the SWCNT walls as described by Pekker *et al.*[38] This hydrogenation is, however, rather mild and nondependent on the type of SWCNTs or their diameter.[39] The D band increased further for the quenched SWCNT polyelectrolytes in contact with DMSO (Figure 4a black and green curves).[40] When SWCNT salts are mixed with DMSO, two phases are formed: a supernatant phase containing the SWCNT polyelectrolyte solution and an undissolved solid phase of SWCNT salts. When the Raman spectra of SWCNTs in the supernatant and residue are compared, the D peaks in the residue are obviously higher than that in the supernatant (when the G peaks are normalized to the same intensity), indicating that the SWCNTs in the residue are slightly more functionalized.

Figure 4b shows the Raman spectra of the radial breathing mode (RBM) region, and the peaks corresponding to various kinds of SWCNTs were assigned according to previous literature reports.[41,42] When the spectra are normalized to the intensity of the (7,6) Raman peak, it is noticeable that the spectra for pristine SWCNTs and quenched SWCNT polyelectrolyte solids are very similar, which is consistent with previous studies of SWCNT polyelectrolytes.[39] However, for the supernatant and residue, there is a dramatic decrease for the (10,2) SWCNT type. A possible explanation for this is that, in DMSO, functionalization happens preferentially to the smaller diameter SWCNT polyelectrolytes. A previous work has been done on the covalent functionalization of SWCNT polyelectrolytes in DMSO, which is fully consistent with what we observe; however, they have not mentioned the selectivity toward small-diameter SWCNTs in their work.[40] Diameter-selective alkylation of SWCNTs has been previously reported.[39,43,44] When SWCNTs were covalently functionalized using alkyl halides and SWCNT polyelectrolyte (Billups' procedure), the peaks corresponding to the smaller diameter SWCNTs decreased or even vanished. The authors attributed this to the preferential functionalization of small-diameter SWCNTs. In our case, the decrease of the Raman (10,2) peak can be attributed to higher functionalization of small

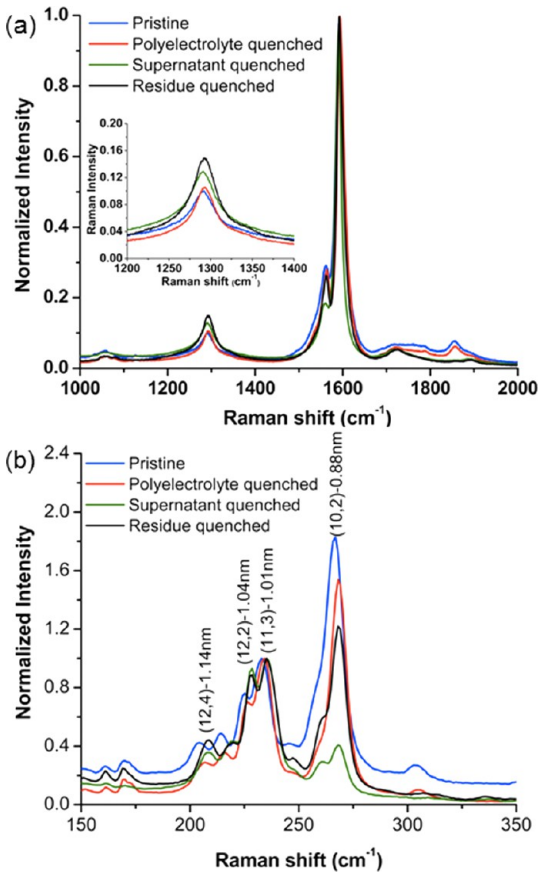

Figure 4. (a) Raman spectra of pristine SWCNTs, SWCNT polyelectrolytes quenched, supernatant quenched, and residue quenched with methanol. (b) Raman spectra of the RBM region of pristine SWCNTs, SWCNT polyelectrolytes quenched, supernatant quenched, and residue quenched with methanol. All spectra were obtained with an excitation wavelength of 785 nm.

diameter tubes. This can be rationalized in terms of the curvature of the SWCNTs, which is more pronounced for SWCNTs with smaller diameter.

It is necessary, however, to point out that conclusions based on the intensity of the (10,2) Raman transition can be influenced by the SWCNT aggregation state. This band is sometimes known as the ``roping peak'' and has been associated with the degree of aggregation of SWCNTs.[45−47] Therefore, the lower intensity of the (10,2) band could be due to a lower degree of entanglement of the SWCNTs quenched from the supernatant. More conclusive evidence for selective SWCNT functionalization can be drawn from photoluminescence spectroscopy as described below.

To verify the debundling of SWCNTs, we also analyzed the Raman tangential mode. A close inspection of the G^- and G^+ peaks indicates that there are no pronounced displacements, which is predictable since the materials have been fully quenched and no doping is expected. However, we did see differences for the line width Γ (full width at half-maximum (fwhm)) of the G^+ peaks. The Γ_{G^+} value for pristine SWCNTs (25 cm^{-1}) is larger than polyelectrolyte-quenched (20 cm^{-1}), residue-quenched (18 cm^{-1}), and supernatant-quenched (15 cm^{-1}). This can be explained due to the increasing degree of debundling after the reaction and dispersion,[48] which can also well fit the result observed for the (10,2) peak in the RBM region. On the other hand, the maximum change in the line width of the G^- peaks is 1−2 cm^{-1}, which is in the margin of the instrumental broadening.[48,49]

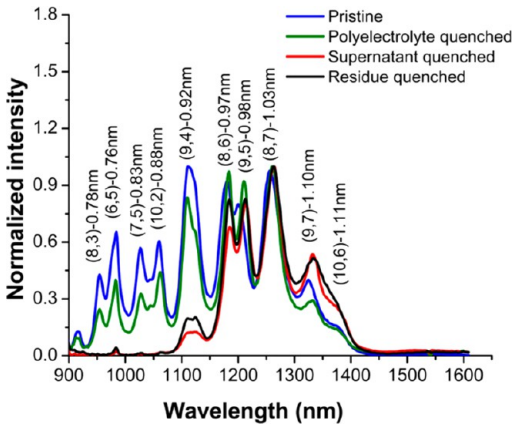

Figure 5. Photoluminescence spectra (785 nm excitation) of pristine SWCNTs, as well as SWCNT polyelectrolyte solids, SWCNT supernatant in DMSO, and residue quenched with methanol and redispersed in SDBS aqueous solution.

Photoluminescence spectroscopy was used as an additional characterization method. Semiconducting SWCNTs display photoluminescence with energies according to their band gap. SWCNT polyelectrolytes were quenched with methanol and redispersed in aqueous solution using 1% SDBS. Figure 5 and Figures S7 and S8 in the Supporting Information show the NIR photoluminescence spectra of SWCNT polyelectrolytes after different treatments at three different excitation wavelengths (the peaks were assigned based on previous reports[41,50]). From Figure 5, it is noticeable that the spectra for purified SWCNTs and for the methanol-quenched SWCNT polyelectrolyte solid are similar. Furthermore, it is observed that, for the supernatant and the residue of quenched SWCNT polyelectrolytes in DMSO, the photoluminescence of SWCNTs decreases with the diameter of the tubes. Interestingly, the photoluminescence basically vanished for tubes smaller than 0.88 nm (based in Figures 5, S7, and S8). The reduction of the photoluminescence intensity as the diameter of the SWCNTs decreases is further confirmation that functionalization is favored as the diameter of the SWCNTs decreases.

CONCLUSIONS

We demonstrate that the solubility of HiPco SWCNT polyelectrolytes is dependent on the initial amount of carbon nanotubes used. The concentrations of SWCNT polyelectrolyte solutions in DMSO can be effectively increased by using the potassium cation sequester

18-crown-6. Concentrations as high as 9.4 mg/mL in DMSO can be achieved with an initial amount of SWCNT polyelectrolytes of 11 mg/mL with 20 mg/mL 18-crown-6. We have used UV−vis spectroscopy to determine the concentration of SWCNT polyelectrolytes in DMSO, which has proven to be a rapid and efficient way to determine dispersion concentrations. Furthermore, cross-polarization microscopy was used to confirm that a liquid-crystal phase was formed at concentrations higher that 3.8 mg/mL of SWCNT polyelectrolytes in DMSO. Finally, small-diameter SWCNT polyelectrolytes show preferential functionalization when dispersed with DMSO, which influences the intensity of the peaks in the Raman RBM region and the features in the photoluminescence spectra. The lost of photoluminescence from small diameter SWCNTs is a definite proof of their functionalization.

EXPERIMENTAL SECTION

Materials. The HiPco SWCNTs (product code: 195.1) used in this work were obtained from Rice University and purified by a previous reported procedure.[51] Potassium metal and dimethyl sulfoxide (DMSO) were purchased from Sigma Aldrich. Naphthalene was purchased from Alfa Aesar. All of the reagents above were used as received. 18-Crown-6 was purchased from Acros and purified by recrystallization in dry acetonitrile. Freshly distilled tetrahydrofuran (THF) over Na/benzophenone was used for making the SWCNT polyelectrolytes.

General Procedure for the Preparation of SWCNT Polyelectrolytes. The synthesis of SWCNT polyelectrolytes was performed following a modified method from literature.[21] First, 69.6 mg of potassium metal (1.78 mmol), 163.2 mg of naphthalene (1.27 mmol), and 56 mL of distilled THF were added to a 100 mL round-bottom flask and stirred for 3 days under room temperature until no obvious solid remained. The resulting dark green solution served as stock solution and was used within 24 h. Then, 150 mg of purified HiPco SWCNTs and 24 mL of stock solution were added to a 50 mL round-bottom flask and stirred for 2 days at room temperature. The crude product was filtrated using 0.45 μm PTFE membranes to obtain a black solid SWCNT polyelectrolyte, which was rinsed with distilled THF. The SWCNT polyelectrolyte was dried overnight at room temperature under vacuum. All of the work was done inside a glovebox under a nitrogen atmosphere.

Dispersion of SWCNT Polyelectrolytes. Dry SWCNT polyelectrolytes (10−30 mg) and a calculated volume (according to the initial concentration desired) of DMSO (or crown ether solution in DMSO) were added to an 8 mL glass vial and sealed. The solution was stirred for 14 h to fully disperse the SWCNT polyelectrolyte and centrifuged under 9900*g* for 45 min. The supernatant layers were extracted for analysis.

Determination of the Solubility of SWCNT Polyelectrolytes. The supernatant layers were diluted 100 times in order to make solutions amenable for UV−vis spectroscopy. The absorption at 500 nm was used as a measurable parameter representing the amount of SWCNT polyelectrolyte dispersed. For the exact solubility, 1 mL of the supernatant of different SWCNT polyelectrolyte dispersions was added to preweighed 8 mL vials. Then, the solutions were dried under vacuum in a 100 °C oil bath for 1 day to remove the solvents. The vial with the residue was weighed to get the solubility. The proportionality constant was calculated from the slope of the graph in Figure S1 (Supporting Information) to be 3.23×10^{-3} ppm^{-1} mm^{-1} (0.323 mL/mg mm^{-1}). This proportionality constant was used to calculate the solubilities of all other solutions.

Conflict of Interest: The authors declare no competing financial interest.

Acknowledgment. The authors acknowledge the Welch Foundation grants C-1743 (AAM) and C-1668 (MP). Dr. Natnael Behabtu is acknowledged for helpful discussions concerning the liquid-crystalline phase. Dr. Saunab Ghosh is acknowledged for his help with the NIR photoluminescence of SWCNT.

Supporting Information Available: Absorbance *vs* SWCNT polyelectrolyte concentration calibration curve; UV−vis spectra of different initial concentrations of SWCNTs in DMSO; solubility of SWCNT polyelectrolytes at different concentrations; image of 11 mg/mL SWCNT polyelectrolyte with 20 mg/mL crown ether forming gels after 4 h; polarized optical microscopy of 2.3 mg/mL SWCNT polyelectrolyte solutions and of crown ether; polarized optical microscopy of 4.4 mg/mL SWCNT polyelectrolyte solutions with 20 mg/mL 18-crown-6; photoluminescence spectra (642 nm and 659 nm excitation) of pristine SWCNTs, as well as SWCNT polyelectrolyte solids, SWCNT supernatant in DMSO, and residue quenched with methanol and redispersed in SDBS aqueous solution. This material is available free of charge via the Internet at http://pubs.acs.org.

REFERENCES AND NOTES

1. Wang, C.; Chien, J. C.; Takei, K.; Takahashi, T.; Nah, J.; Niknejad, A. M.; Javey, A. Extremely Bendable, High-Performance Integrated Circuits Using Semiconducting Carbon Nanotube Networks for Digital, Analog, and Radio-Frequency Applications. *Nano Lett.* **2012**, *12*, 1527–1533.
2. Zhao, J. W.; Gao, Y. L.; Lin, J.; Chen, Z.; Cui, Z. Printed Thin-Film Transistors with Functionalized Single-Walled Carbon Nanotube Inks. *J. Mater. Chem.* **2012**, *22*, 2051–2056.
3. Jo, J. W.; Jung, J. W.; Lee, J. U.; Jo, W. H. Fabrication of Highly Conductive and Transparent Thin Films from Single-Walled Carbon Nanotubes Using a New Non-ionic Surfactant *via* Spin Coating. *ACS Nano* **2010**, *4*, 5382–5388.
4. Liu, W. B.; Pei, S. F.; Du, J. H.; Liu, B. L.; Gao, L. B.; Su, Y.; Liu, C.; Cheng, H. M. Additive-Free Dispersion of Single-Walled Carbon Nanotubes and Its Application for Transparent Conductive Films. *Adv. Funct. Mater.* **2011**, *21*, 2330–2337.
5. Saha, A.; Ghosh, S.; Weisman, R. B.; Martí, A. A. Films of Bare Single-Walled Carbon Nanotubes from Superacids with Tailored Electronic and Photoluminescence Properties. *ACS Nano* **2012**, *6*, 5727–5734.
6. Mirri, F.; Ma, A. W. K.; Hsu, T. T.; Behabtu, N.; Eichmann, S. L.; Young, C. C.; Tsentalovich, D. E.; Pasquali, M. High-Performance Carbon Nanotube Transparent Conductive Films by Scalable Dip Coating. *ACS Nano* **2012**, *6*, 9737–9744.
7. Holt, J. M.; Ferguson, A. J.; Kopidakis, N.; Larsen, B. A.; Bult, J.; Rumbles, G.; Blackburn, J. L. Prolonging Charge Separation in P3HT−SWNT Composites Using Highly Enriched Semiconducting Nanotubes. *Nano Lett.* **2010**, *10*, 4627–4633.
8. Ren, S. Q.; Bernardi, M.; Lunt, R. R.; Bulovic, V.; Grossman, J. C.; Gradecak, S. Toward Efficient Carbon Nanotube/P3HT Solar Cells: Active Layer Morphology, Electrical, and Optical Properties. *Nano Lett.* **2011**, *11*, 5316–5321.
9. Ramesh, S.; Ericson, L. M.; Davis, V. A.; Saini, R. K.; Kittrell, C.; Pasquali, M.; Billups, W. E.; Adams, W. W.; Hauge, R. H.; Smalley, R. E. Dissolution of Pristine Single Walled Carbon Nanotubes in Superacids by Direct Protonation. *J. Phys. Chem. B* **2004**, *108*, 8794–8798.
10. Girifalco, L. A.; Hodak, M.; Lee, R. S. Carbon Nanotubes, Buckyballs, Ropes, and a Universal Graphitic Potential. *Phys. Rev. B* **2000**, *62*, 13104–13110.
11. Chen, Z.; Kobashi, K.; Rauwald, U.; Booker, R.; Fan, H.; Hwang, W.-F.; Tour, J. M. Soluble Ultra-short Single-Walled

Carbon Nanotubes. *J. Am. Chem. Soc.* **2006**, *128*, 10568–10571.
12. Gebhardt, B.; Hof, F.; Backes, C.; Muller, M.; Plocke, T.; Maultzsch, J.; Thomsen, C.; Hauke, F.; Hirsch, A. Selective Polycarboxylation of Semiconducting Single-Walled Carbon Nanotubes by Reductive Sidewall Functionalization. *J. Am. Chem. Soc.* **2011**, *133*, 19459–19473.
13. Strano, M. S.; Dyke, C. A.; Usrey, M. L.; Barone, P. W.; Allen, M. J.; Shan, H.; Kittrell, C.; Hauge, R. H.; Tour, J. M.; Smalley, R. E. Electronic Structure Control of Single-Walled Carbon Nanotube Functionalization. *Science* **2003**, *301*, 1519–1522.
14. Tuncel, D. Non-Covalent Interactions between Carbon Nanotubes and Conjugated Polymers. *Nanoscale* **2011**, *3*, 3545–3554.
15. Jain, D.; Saha, A.; Marti, A. A. Non-covalent Ruthenium Polypyridyl Complexes-Carbon Nanotubes Composites: An Alternative for Functional Dissolution of Carbon Nanotubes in Solution. *Chem. Commun.* **2011**, *47*, 2246–2248.
16. Li, H.; Zhou, B.; Lin, Y.; Gu, L.; Wang, W.; Fernando, K. A. S.; Kumar, S.; Allard, L. F.; Sun, Y.-P. Selective Interactions of Porphyrins with Semiconducting Single-Walled Carbon Nanotubes. *J. Am. Chem. Soc.* **2004**, *126*, 1014–1015.
17. Rai, P. K.; Pinnick, R. A.; Parra-Vasquez, A. N. G.; Davis, V. A.; Schmidt, H. K.; Hauge, R. H.; Smalley, R. E.; Pasquali, M. Isotropic–Nematic Phase Transition of Single-Walled Carbon Nanotubes in Strong Acids. *J. Am. Chem. Soc.* **2006**, *128*, 591–595.
18. Davis, V. A.; Parra-Vasquez, A. N. G.; Green, M. J.; Rai, P. K.; Behabtu, N.; Prieto, V.; Booker, R. D.; Schmidt, J.; Kesselman, E.; Zhou, W.; *et al.* True Solutions of Single-Walled Carbon Nanotubes for Assembly into Macroscopic Materials. *Nat. Nanotechnol.* **2009**, *4*, 830–834.
19. Saha, A.; Ghosh, S.; Behabtu, N.; Pasquali, M.; Marti, A. A. Single-Walled Carbon Nanotubes Shell Decorating Porous Silicate Materials: A General Platform for Studying the Interaction of Carbon Nanotubes with Photoactive Molecules. *Chem. Sci.* **2011**, *2*, 1682–1687.
20. Pénicaud, A.; Poulin, P.; Derré, A.; Anglaret, E.; Petit, P. Spontaneous Dissolution of a Single-Wall Carbon Nanotube Salt. *J. Am. Chem. Soc.* **2004**, *126*, 8–9.
21. Voiry, D.; Roubeau, O.; Penicaud, A. Stoichiometric Control of Single Walled Carbon Nanotubes Functionalization. *J. Mater. Chem.* **2010**, *20*, 4385–4391.
22. Voiry, D.; Drummond, C.; Penicaud, A. Portrait of Carbon Nanotube Salts as Soluble Polyelectrolytes. *Soft Matter* **2011**, *7*, 7998–8001.
23. Petit, P.; Mathis, C.; Journet, C.; Bernier, P. Tuning and Monitoring the Electronic Structure of Carbon Nanotubes. *Chem. Phys. Lett.* **1999**, *305*, 370–374.
24. Liang, F.; Sadana, A. K.; Peera, A.; Chattopadhyay, J.; Gu, Z. N.; Hauge, R. H.; Billups, W. E. A Convenient Route to Functionalized Carbon Nanotubes. *Nano Lett.* **2004**, *4*, 1257–1260.
25. Ko, H.; Tsukruk, V. V. Liquid-Crystalline Processing of Highly Oriented Carbon Nanotube Arrays for Thin-Film Transistors. *Nano Lett.* **2006**, *6*, 1443–1448.
26. Ericson, L. M.; Fan, H.; Peng, H.; Davis, V. A.; Zhou, W.; Sulpizio, J.; Wang, Y.; Booker, R.; Vavro, J.; Guthy, C.; *et al.* Macroscopic, Neat, Single-Walled Carbon Nanotube Fibers. *Science* **2004**, *305*, 1447–1450.
27. Penicaud, A.; Valat, L.; Derre, A.; Poulin, P.; Zakri, C.; Roubeau, O.; Maugey, M.; Miaudet, P.; Anglaret, E.; Petit, P.; *et al.* Mild Dissolution of Carbon Nanotubes: Composite Carbon Nanotube Fibres from Polyelectrolyte Solutions. *Compos. Sci. Technol.* **2007**, *67*, 795–797.
28. Behabtu, N.; Young, C. C.; Tsentalovich, D. E.; Kleinerman, O.; Wang, X.; Ma, A. W. K.; Bengio, E. A.; ter Waarbeek, R. F.; de Jong, J. J.; Hoogerwerf, R. E.; *et al.* Strong, Light, Multifunctional Fibers of Carbon Nanotubes with Ultrahigh Conductivity. *Science* **2013**, *339*, 182–186.
29. Wilkinson, T. D.; Wang, X.; Teo, K. B. K.; Milne, W. I. Sparse Multiwall Carbon Nanotube Electrode Arrays for Liquid-Crystal Photonic Devices. *Adv. Mater.* **2008**, *20*, 363–366.
30. Zhang, S.; Kinloch, I. A.; Windle, A. H. Mesogenicity Drives Fractionation in Lyotropic Aqueous Suspensions of Multiwall Carbon Nanotubes. *Nano Lett.* **2006**, *6*, 568–572.
31. Zhang, S. J.; Kumar, S. CarbonNanotubes as Liquid Crystals. *Small* **2008**, *4*, 1270–1283.
32. Parra-Vasquez, A. N. G.; Behabtu, N.; Green, M. J.; Pint, C. L.; Young, C. C.; Schmidt, J.; Kesselman, E.; Goyal, A.; Ajayan, P. M.; Cohen, Y.; *et al.* Spontaneous Dissolution of Ultralong Single- and Multiwalled Carbon Nanotubes. *ACS Nano* **2010**, *4*, 3969–3978.
33. Davis, V. A.; Ericson, L. M.; Parra-Vasquez, A. N. G.; Fan, H.; Wang, Y.; Prieto, V.; Longoria, J. A.; Ramesh, S.; Saini, R. K.; Kittrell, C.; *et al.* Phase Behavior and Rheology of SWNTs in Superacids. *Macromolecules* **2003**, *37*, 154–160.
34. Moore, V. C.; Strano, M. S.; Haroz, E. H.; Hauge, R. H.; Smalley, R. E.; Schmidt, J.; Talmon, Y. Individually Suspended Single-Walled Carbon Nanotubes in Various Surfactants. *Nano Lett.* **2003**, *3*, 1379–1382.
35. Pedersen, C. J. Cyclic Polyethers and Their Complexes with Metal Salts. *J. Am. Chem. Soc.* **1967**, *89*, 7017–7036.
36. Pedersen, C. J. Crystalline Salt Complexes of Macrocyclic Polyethers. *J. Am. Chem. Soc.* **1970**, *92*, 386–391.
37. Pedersen, C. J.; Frensdorff, H. K. Macrocyclic Polyethers and Their Complexes. *Angew. Chem., Int. Ed.* **1972**, *11*, 16–25.
38. Pekker, S.; Salvetat, J. P.; Jakab, E.; Bonard, J. M.; Forró, L. Hydrogenation of Carbon Nanotubes and Graphite in Liquid Ammonia. *J. Phys. Chem. B* **2001**, *105*, 7938–7943.
39. Wunderlich, D.; Hauke, F.; Hirsch, A. Preferred Functionalization of Metallic and Small-Diameter Single Walled Carbon Nanotubes *via* Reductive alkylation. *J. Mater. Chem.* **2008**, *18*, 1493–1497.
40. Guan, J. W.; Martinez-Rubi, Y.; Denommee, S.; Ruth, D.; Kingston, C. T.; Daroszewska, M.; Barnes, M.; Simard, B. About the Solubility of Reduced SWCNT in DMSO. *Nanotechnology* **2009**, *20*, 245701.
41. Bachilo, S. M.; Strano, M. S.; Kittrell, C.; Hauge, R. H.; Smalley, R. E.; Weisman, R. B. Structure-Assigned Optical Spectra of Single-Walled Carbon Nanotubes. *Science* **2002**, *298*, 2361–2366.
42. Araujo, P. T.; Pesce, P. B. C.; Dresselhaus, M. S.; Sato, K.; Saito, R.; Jorio, A. Resonance Raman Spectroscopy of the Radial Breathing Modes in Carbon Nanotubes. *Physica E* **2010**, *42*, 1251–1261.
43. Müller, M.; Maultzsch, J.; Wunderlich, D.; Hirsch, A.; Thomsen, C. Diameter Dependence of Addition Reactions to Carbon Nanotubes. *Phys. Status Solidi B* **2008**, *245*, 1957–1960.
44. Hodge, S. A.; Bayazit, M. K.; Coleman, K. S.; Shaffer, M. S. P. Unweaving the Rainbow: A Review of the Relationship between Single-Walled Carbon Nanotube Molecular Structures and Their Chemical Reactivity. *Chem. Soc. Rev.* **2012**, *41*, 4409–4429.
45. Heller, D. A.; Barone, P. W.; Swanson, J. P.; Mayrhofer, R. M.; Strano, M. S. Using Raman Spectroscopy To Elucidate the Aggregation State of Single-Walled Carbon Nanotubes. *J. Phys. Chem. B* **2004**, *108*, 6905–6909.
46. O'Connell, M. J.; Sivaram, S.; Doorn, S. K. Near-Infrared Resonance Raman Excitation Profile Studies of Single-Walled Carbon Nanotube Intertube Interactions: A Direct Comparison of Bundled and Individually Dispersed HiPco Nanotubes. *Phys. Rev. B* **2004**, *69*, 235415.
47. Luo, Z.; Doorn, S. K.; Li, R.; Papadimitrakopoulos, F. Effects of Aggregation and Electron–Phonon Interactions on RBM Spectral Reconstruction of Single Walled Carbon Nanotubes. *Phys. Status Solidi B* **2006**, *243*, 3155–3160.
48. Jorio, A.; Fantini, C.; Dantas, M. S. S.; Pimenta, M. A.; Souza Filho, A. G.; Samsonidze, G. G.; Brar, V. W.; Dresselhaus, G.; Dresselhaus, M. S.; Swan, A. K.; *et al.* Linewidth of the Raman Features of Individual Single-Wall Carbon Nanotubes. *Phys. Rev. B* **2002**, *66*, 115411.
49. Cardenas, J. F.; Gromov, A. The Effect of Bundling on the G′ Raman Band of Single-Walled Carbon Nanotubes. *Nanotechnology* **2009**, *20*, 465703.

50. Weisman, R. B.; Bachilo, S. M. Dependence of Optical Transition Energies on Structure for Single-Walled Carbon Nanotubes in Aqueous Suspension: An Empirical Kataura Plot. *Nano Lett.* **2003**, *3*, 1235–1238.
51. Chiang, I. W.; Brinson, B. E.; Huang, A. Y.; Willis, P. A.; Bronikowski, M. J.; Margrave, J. L.; Smalley, R. E.; Hauge, R. H. Purification and Characterization of Single-Wall Carbon Nanotubes (SWNTs) Obtained from the Gas-Phase Decomposition of CO (HiPco Process). *J. Phys. Chem. B* **2001**, *105*, 8297–8301.